Published OnlineFirst February 18, 2015; DOI: 10.1158/1535-7163.MCT-14-0970

Models and Technologies

Molecular Cancer Therapeutics

RNA Interference Using *c-Myc*–Conjugated Nanoparticles Suppresses Breast and Colorectal Cancer Models

Naveen K. Tangudu[1], Vinod K. Verma[1], Tristan D. Clemons[2], Syed S. Beevi[1], Trevor Hay[3], Ganesh Mahidhara[1], Meera Raja[3], Rekha A. Nair[4], Liza E. Alexander[4], Anant B. Patel[1], Jedy Jose[1], Nicole M. Smith[5], Bogdan Zdyrko[6], Anne Bourdoncle[5], Igor Luzinov[6], K. Swaminathan Iyer[2], Alan R. Clarke[3], and Lekha Dinesh Kumar[1]

Abstract

In this article, we report the development and preclinical validation of combinatorial therapy for treatment of cancers using RNA interference (RNAi). RNAi technology is an attractive approach to silence genes responsible for disease onset and progression. Currently, the critical challenge facing the clinical success of RNAi technology is in the difficulty of delivery of RNAi inducers, due to low transfection efficiency, difficulties of integration into host DNA and unstable expression. Using the macromolecule polyglycidal methacrylate (PGMA) as a platform to graft multiple polyethyleneimine (PEI) chains, we demonstrate effective delivery of small oligos (anti-miRs and mimics) and larger DNAs (encoding shRNAs) in a wide variety of cancer cell lines by successful silencing/activation of their respective target genes. Furthermore, the effectiveness of this therapy was validated for *in vivo* tumor suppression using two transgenic mouse models; first, tumor growth arrest and increased animal survival was seen in mice bearing *Brca2*/*p53*-mutant mammary tumors following daily intratumoral treatment with nanoparticles conjugated to *c-Myc* shRNA. Second, oral delivery of the conjugate to an *Apc*-deficient crypt progenitor colon cancer model increased animal survival and returned intestinal tissue to a non–*wnt*-deregulated state. This study demonstrates, through careful design of nonviral nanoparticles and appropriate selection of therapeutic gene targets, that RNAi technology can be made an affordable and amenable therapy for cancer. *Mol Cancer Ther; 14(5); 1259–69. ©2015 AACR.*

Introduction

Cancer is a major global health problem and is a leading cause of death both in developed and developing countries. Most commonly practiced therapies in patients target cancer cells by the use of nonspecific and nonselective treatments that cause significant off-target effects. In particular, chemotherapy is the preferred clinical method for cancer treatment since the 1940s, despite its many side effects. Biologic therapies are in limited use in augmenting standard therapies, but this approach has thus far not been effective enough to replace the traditional methods of chemotherapy in the majority of cancers. The shortcomings in efficacy and safety associated with the current treatment regimens emphasize the need for highly specific and targeted alternative therapies that could maximize patient survival and minimize the limitations of the existing strategies.

The discovery of the *c-Myc* gene has changed our fundamental understanding of malignancy and it is now well established that c-Myc is deregulated in the majority of cancers (1). Mechanistically, the basis of this association appears to stem from the plethora of roles played by *c-Myc* in regulating cell death, growth, and proliferation, as well as in regulating important biochemical functions such as the uptake and metabolism of cellular glucose (2). *c-Myc* therefore appears to act as a cellular master switch, controlling a network of oncogenes and tumor suppressor genes through a variety of signal transduction pathway molecules. Mutations in *c-Myc* or gross changes in its expression levels, clearly have the potential to derail the otherwise precise checkpoints that maintain cells in their normal quiescent state and lead to the development of cancer. Therapeutically, approaches that would allow the reprogramming and retuning of *c-Myc* activity within cancer cells are attractive strategies for disease control and

[1]Cancer Biology, Centre for Cellular and Molecular Biology, Council of Scientific and Industrial Research, Hyderabad, India. [2]School of Chemistry and Biochemistry, The University of Western Australia, Crawley, Australia. [3]European Cancer Stem Cell Research Institute, Cardiff University, Cathays, Cardiff, United Kingdom. [4]Department of Pathology, Regional Cancer Centre, Trivandrum, India. [5]Univ de Bordeaux, INSERM U869, IECB, ARNA Laboratory, Pessac, France. [6]School of Materials Science and Engineering, Clemson University, Clemson, South Carolina.

Note: Supplementary data for this article are available at Molecular Cancer Therapeutics Online (http://mct.aacrjournals.org/).

N.K. Tangudu and V.K. Verma contributed equally to this article.

T.D. Clemons and S.S. Beevi contributed equally to this article.

Corresponding Authors: Lekha Dinesh Kumar, Cancer Biology, Centre for Cellular and Molecular Biology, Hyderabad, Andhra Pradesh 500007, India. Phone: 9140-2719-2933, ext. 2576; Fax: 9140-2716-0591; E-mail: lekha@ccmb.res.in; Swaminathan Iyer, BioNano UWA, School of Chemistry and Biochemistry, Mailbag M310, Faculty of Sciences, The University of Western Australia, 35 Stirling Highway, Crawley, Western Australia 6009. Phone: 618-6488-4470; Fax: 618-6488-7330; E-mail: swaminatha.iyer@uwa.edu.au; and Alan R. Clarke, European Cancer Stem Cell Research Institute, (ECSCRI), Cardiff CR-UK Centre, Cardiff School of Biosciences, Cardiff University, Hadyn Ellis Building, Maindy Road, Cathays, Cardiff CF24 4HQ, United Kingdom. Phone: 4402-9208-74609, Fax: 4402-9208-74116; E-mail: ClarkeAR@cf.ac.uk

doi: 10.1158/1535-7163.MCT-14-0970

Published OnlineFirst February 18, 2015; DOI: 10.1158/1535-7163.MCT-14-0970

prevention (3). One such approach is the use of RNA interference (RNAi) technology. Recent breakthroughs in RNAi technology have vastly improved our understanding of how gene expression can be specifically modulated and can be employed as a potential therapeutic tool (4–7). Harnessing small RNA molecules to silence genes involved in the development and growth of cancer cells is an important step forward in developing a new and target-focused cancer therapy (8). The biggest challenge to the use of RNAi technology lies in achieving effective intracellular delivery of therapeutic molecules, in the form of either siRNA or short hairpin RNA (shRNA; ref. 9). Recently, spherical nucleic acid-gold nanoparticle conjugates were shown to cross the blood–brain barrier and induce apoptosis in glioma cells, thereby reducing tumor burden (10). While the preformed 21 base siRNA duplexes are highly unstable, with a transient period of expression, shRNAs are more robust and better suited for long-term effectiveness, due to their ability to produce siRNAs continuously within the cell and hence bring about prolonged knockdown of the target genes. Although a shRNA-based approach would be ideal for cancer-related therapeutic development, they have thus far only been delivered effectively *in vivo* using viral vectors. However, with viral-based delivery, it is important to bear in mind their potential immunogenicity and the risk of becoming pathogenic due to mutations. The idea of using a nonviral agent stems from its ability to mimic a viral function to infect cells, while avoiding the dangers of virus-associated pathogenesis. The use of nonviral transfecting agents has been proposed for several years because they are theoretically safer and easier to produce (11). However, their clinical success has been limited in the delivery of shRNA due to low transfection efficiency, difficulties of integration, and unstable expression.

Currently, polyethyleneimine (PEI) is the most widely used nonviral agent and is considered the gold standard *in vitro* (12). The major drawback of PEI as a transfecting agent is its cytotoxicity, and the observed correlation between increased transfection efficacy with increased molecular weight and concentration of PEI (13–16) makes it a difficult proposition to improve efficiency without its deleterious effect on cells. We have previously demonstrated that anchoring multiple PEI chains to PGMA nanoparticles can dramatically decrease their toxicity even at higher concentrations, while achieving efficient nanoparticle endocytosis (17). In the current study, various types of nucleic acids, designed to target cancer-related genes, were tested in different cancer cell lines after conjugation to these nanoparticles. shRNAs of *c-Myc* oncogene were selected to test the *in vivo* efficacy of this biologic drug complex in targeting knockdown of the oncogene and related signaling cascades, thus triggering suppression of growth in established mouse models of colorectal and breast cancer.

Materials and Methods

Preparation and characterization of the PEI-PGMA nanoparticles

The PEI-PGMA nanoparticles were prepared following the procedure outlined by Evans and colleagues (16) with the magnetic cores synthesized as per the procedure outlined by Sun and colleagues (18). The nanoparticles were characterized using TEM (JOEL 2100) at 120 kV, dynamic light scattering for size and surface charge, and fluorescence spectrometry. Nitrogen concentration was obtained using elemental analysis of the nanoparticles before and after PEI attachment. Nitrogen concentration was determined to be 765 μmol/L at a nanoparticle concentration of 1 mg/mL. The nanoparticles were superparamagnetic as determined by SQUID magnetometry, as there was no hysteresis at 300K (with specific saturation magnetization of 6 emu/g), and the relaxivity r^2 of the nanoparticle was determined, based on the iron content inside the polymer, to be 340 per s × (mmol/L) Fe. The nanoparticles were centrifuged (16,000 × *g*, 30 minutes), the supernatant was removed and the nanoparticle pellet was resuspended in 20 mmol/L HEPES buffer containing 150 mmol/L NaCl. They were then sterilized under UV for 20 minutes and mixed with DNA in different ratios and incubated at room temperature for 45 minutes. To assess optimal binding, a gel retardation assay was performed for the different ratios (W/V) of PEI-PGMA (nanoparticles) with short oligos and plasmid DNA (D; N:D ratio). It was determined that the ratio of (N:D) 4:1 and 25:1 were optimal for binding oligos and plasmid DNA, respectively. The appropriate ratios (N:D) were determined as 4:1 for oligos and 25:1 for larger DNA molecules. This ratio was maintained throughout the study.

In vitro transfection studies

Adherent HEK293 (Human Embryonic Kidney), MCF7, and MDA-MB231 (breast cancer), semiadherent COLO205 (colon cancer), and nonadherent Jurkat (Leukemia) cell lines were obtained from ATCC. The cells were 4 to 6 months old at the time of experimentation and mycoplasma testing (Look out mycoplasma PCR detection Kit, Sigma) was performed regularly and assured that these cell lines are free of mycoplasma. DNA constructs used were GIPZ *c-Myc* shRNA Transfection Starter Kit (RHS4287-EG17869) and GIPZ nonsilencing shRNA (RHS4346), which was used as negative control to rule out off-target effects (Open Biosystems). In the case of the shRNAs, the best out of the four that showed maximum knockdown was selected for *in vivo* experiments. Mimics and anti-miRs were purchased from Exiqon. Cells were seeded in complete media (RPMI for Jurkat and DMEM for all other cell lines, with 10% FBS) in 24-well plates in triplicates at a density of 2×10^5 cells/mL for all transfection studies. After 12 to 24 hours, 50% to 60% confluent cells were transfected with DNA/RNA nanoparticle complex in the above stated ratios, depending on the types of DNA/RNA used. The complexes were incubated at 37°C for 4 hours (small oligos) and 6 hours (for larger plasmids), replaced with fresh complete media and incubated in a CO_2-regulated incubator for another 48 or 72 hours for qPCR or immunoblot analysis, respectively. The transfection with Lipofectamine 2000 (Invitrogen) was performed in an identical manner to that of the nanoparticles. All the experiments were repeated a minimum of three times for statistical analysis.

For immunocytochemistry (ICC), cells were seeded on a coverslip in triplicates at the rate of 2×10^5 cells/mL and the transfected cells were fixed with 4% formaldehyde diluted in PBS. Fixed cells were permeabilized by incubation with 0.5% Triton X-100 in PBS for 10 minutes. After blocking with 10% normal goat serum in PBS for 1 hour, cells were incubated overnight at 4°C with either the rabbit monoclonal anti-*p53*, anti-*c-Myc* (Millipore), or anti-GAPDH antibodies (Calbiochem) at 1:200 dilution. These were then washed four times with PBS for 10 minutes each. The cells were subsequently incubated with appropriate secondary antibody conjugated with Alexa 633,488 (Invitrogen) at 1:400 dilutions for 1 hour

Published OnlineFirst February 18, 2015; DOI: 10.1158/1535-7163.MCT-14-0970

at room temperature. Following a further set of four 10-minute washes with PBS, the cells were mounted on DAPI-mounting media containing antifade (Vectashield, Vector Labs). Confocal images were obtained on Leica laser scanning microscope at 63× magnification. Transfection efficiency was performed in triplicates and calculated. One hundred cells were counted per field of view for a total of 4 fields per experiment, per treatment. All experiments were repeated three to five times and data transformed using arcsine transformation method before statistical analysis.

RNA isolation and quantitative real-time PCR analysis

At the end of each timepoint, media were removed and cells were scraped off in TRIzol reagent (Invitrogen). RNA from homogenized tissue samples as well as cell lysates were isolated using RNAeasy Kit (Qiagen) and RNA concentrations were measured using nanodrop spectrometer (Thermo Scientific). A 260/280 nm absorption ratio of 2.0 confirmed the RNA to be pure and protein free. The quality of RNA was also checked using 1% agarose gel electrophoresis. One microgram of total RNA (DNase-treated) was transcribed to cDNA using RT-PCR Reagents Kit (Applied Biosystems) and further used for both SYBR Green assay and Taqman gene expression assay of all the genes. Quantitative PCR analysis was performed using SYBR Green PCR master mix following standard MIQE protocols as well as TaqMan Gene Expression Assays (Applied Biosystems), following the manufacturer's instructions, and the reactions were carried out in a 7900HT Thermo Cycler (Applied Biosystems). TaqMan Gene Expression Assays included a pair of unlabeled PCR primers and a TaqMan probe with a FAM dye label on the 5′ end and minor groove binder (MGB) and nonfluorescent quencher (NFQ) on the 3′ end. 18S rRNA, β-actin, and nono genes were used as endogenous controls to normalize the data (Supplementary Table S1). The fold expressions of particular genes are represented as $\log_{10} 2^{-\Delta\Delta C_t}$. Real-time StatMiner Software was used for data analysis. This software performs parametric, nonparametric, and paired tests for relative quantification of gene expression, as well as a two-way ANOVA for two-factor differential expression analysis.

Immunoblot analysis

Total cellular protein from all cell lines transfected with respective miRNA mimics/knockdown and shRNAs was extracted after 72 hours using lysis buffer containing 1× protease inhibitor cocktail (Calbiochem). Protein concentrations were measured by the Bradford (Sigma) method and equal amounts (~25–30 μg) of cellular extract/lysate were separated on 10%–12% SDS-PAGE gels and electrotransferred onto nitrocellulose membranes (Millipore). Membranes were blocked with 5% non-fat milk for 1 hour at room temperature, before incubation with appropriate primary antibodies for *c-Myc*, *β-catenin*, GAPDH, *p53*, or *β-actin* (1:3,000) overnight at 4°C. Membranes were then incubated with 1:10,000 horseradish peroxidase-conjugated secondary antibody for 1 hour, washed, and signal visualized with ECL plus reagent following exposure onto X-ray film. Anti-human and anti-mouse primary antibodies raised in rabbit were used with a dilution of 1:4,000 for all the Western blot analyses and 1:50 for ICC. The anti-rabbit secondary antibodies raised in goat/donkey were used with a dilution factor of 1:10,000 for Western blot analysis and 1:200 for ICC.

***In vivo* studies**

All animal models were used strictly in accordance with the animal ethical committees of the participating institutes, Centre for Cellular and Molecular Biology (Council of Scientific and Industrial Research, Hyderabad, India), and Cardiff University (Cardiff, United Kingdom), and were housed in the transgenic facilities of the respective institutes. Two types of animal models were used in the study. The breast cancer model (conditional *Brca2*/*p53* knockout under control of *Blg-cre* transgene) develops autochthonous tumors on any of the 5 pairs of mammary glands in a 6- to 15-month time window. PCR conditions for genotyping of the *Blg-cre* transgene and the conditional alleles for *Brca2* and *p53* have already been described (19). Mammary tumors were measured at 0.5 cm^3 before starting treatment and all tumors in each cohort were treated identically by giving intratumoral injections of 10 μg of *c-Myc* DNA (GIPZ *c-Myc* shRNA-vector vehicle, Open Biosystems) complexed with 250 μg of nanoparticles (PEI-PGMA; in a volume of 100 μL) along with the control cohorts (*c-Myc* shRNA alone, scrambled + nanoparticles, nanoparticle alone, untreated). All tumors of a single mouse were given identical treatment and tumors of similar size were taken into consideration while transforming the data. The *Apc* knockout model (*AhCre-ErT* $Apc^{fl/fl}$) is an inducible colorectal cancer model which develops a *c-Myc*–dependent "crypt progenitor" phenotype in the intestine upon injection with β-naphthoflavone and 4-hydroxy tamoxifen (4-OHT), causing death within a few days of induction (20). The *cre* and *Apc* alleles were brought together by extensive breeding and genotyping performed using the primers stated in Supplementary Table S2. Six- to 8-week-old mice were intraperitoneally injected with 80 mg/kg β-naphthoflavone and tamoxifen (dissolved together in corn oil at 10 mg/mL each) once daily for 5 days to cause recombination of the targeted alleles. *Apc* knockout mice were treated with a daily oral dose of 50 μg *c-Myc* shRNA (in pGIPZ vector)-encoding plasmid DNA complexed to 1.25 mg nanoparticles (in a total volume of 250 μL) from day 1 of induction until the end time point as described above. WT refers to healthy wild-type mice (C57/BL6) where control tissues were harvested for comparison with treated mice in all experiments.

Fourier transform infrared spectroscopy

To analyze the toxicity of the nanoparticles *in vivo*, mice were divided into 4 groups consisting of 5 mice each. The different cohorts received 0, 250, 500, or 1,000 μg daily dose of nanoparticles by oral gavage for a period of 21 days in this subchronic toxicity study. The control cohort (no nanoparticles) was treated with just buffer. Following treatment, animals were sacrificed as per the ethics guidelines and tissues (liver, kidney, lung, spleen) were removed and immediately frozen in liquid nitrogen. They were freeze-dried using a Labconco system and crushed under aseptic conditions. The freeze-dried pellets were analyzed for the characteristic peaks that represent intactness of macromolecular organization in the organs. Scanning was performed using a Bruker Vertex-70 FTIR spectrometer, with the ATR mode in the range of 400 to 4,000 per cm to obtain the characteristic peaks.

***In vitro* cytotoxicity assay of PEI-PGMA-nanoparticles**

Adherent (HEK293, MCF7, and MDA-MB231), semiadherent (COLO205), and nonadherent (Jurkat) cells were obtained from ATCC and maintained in the recommended growth media. *In vitro* cytotoxicity of PEI-PGMA-NPs was analyzed by MTT assay. Briefly,

Published OnlineFirst February 18, 2015; DOI: 10.1158/1535-7163.MCT-14-0970

cells were seeded in 96-well plate at a concentration of 2×10^4 cells/well in 100 μL volume, and incubated overnight at 37°C in a humidified atmosphere containing 5% CO_2. Cells were treated with predetermined concentrations (0–300 μg/mL) PEI-PGMA-NP diluted appropriately with culture media in triplicates and grown as above for 48 hours. After the treatment, media containing PEI-PGMA-NP were carefully removed by aspiration. Hundred microliters of 0.4 mg/mL MTT in PBS was added to each well and incubated in the dark for 4 hours. After the incubation period, formazan crystals were solubilized by the addition of 100 μL of DMSO to each well and kept in an incubator for 45 minutes. Amounts of formazan were determined by measuring the absorbance at 540 nm. The data were presented as percentage post-treatment recovery (% live cells), whereas the absorbance from nontreated control cells was defined as 100% live cells. The percentage recovery (% live cells) was plotted against the concentration of PEI-NP. Cells grown in normal growth medium without treatment served as control. Measurements were made in triplicate, and the experiments were repeated thrice with 3 biologic replicates. The signal to background ratio was calculated using the formula S/B = mean signal/mean background. Student one-tailed test was used to determine the statistical significance of the treated versus untreated cells and the error bars represent SD.

Statistical analysis

The data of percentage cells transfected were subjected to arsine transformation, as the values ranged from 4% to 98% and the transformed data were subjected to statistical analysis as per the factorial completely randomized design, with cell type taken as one factor and transfection agent type taken as the other. *In vivo* data obtained are shown as mean values ± SEM. Significant difference between means were performed using two-tailed Student *t* test. *N* is the number of independent animals used in all cases with $P < 0.05$.

Results

Cytotoxicity and biodistribution studies did not show nanoparticle toxicity effects *in vitro* or *in vivo*

The ability of a nonviral transfection agent (Fig. 1A and Supplementary Fig. S1) to bind plasmid DNA, and in turn induce RNAi efficiently, is primarily governed by its ability to successfully bind nucleic acids (RNAs, small oligos, and plasmid DNA encoding shRNAs) at high loading concentrations. Using gel retardation assays, the ratios [PEI-PGMA(N): DNA(D)] of 4:1 and 25:1 [weight/volume (W/V)] were found to be optimum for binding oligos and plasmid DNAs, respectively. These ratios were ideal for

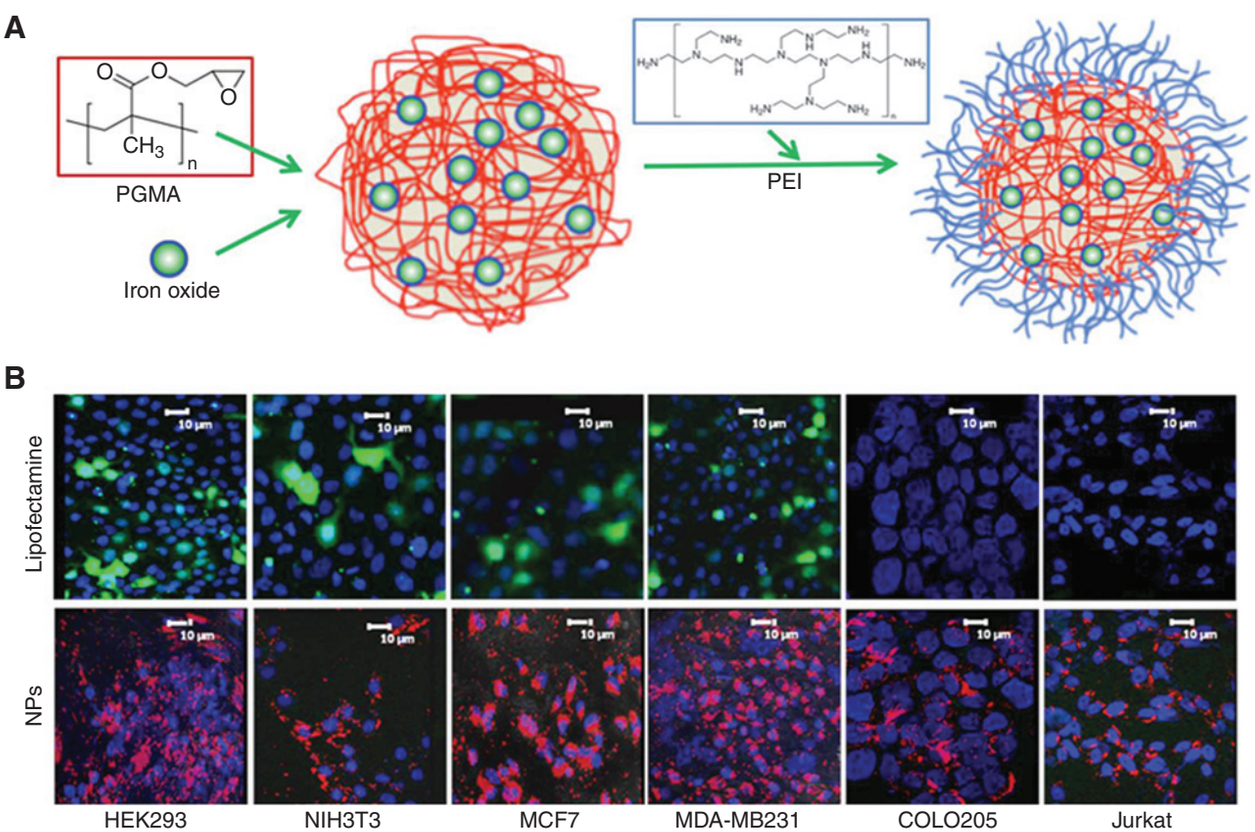

Figure 1.
Comparison of transfection efficiencies of Lipofectamine and PEI-PGMA nanoparticles (NP) in adherent, semiadherent, and nonadherent cell lines. A, schematic representation of the multimodal nanoparticles formed by covalently binding multiple PEI chains on a macromolecular PGMA-RhB modified core. B, representative confocal merged images of various cell lines transfected with the plasmid DNA vector encoding GFP reporter gene using Lipofectamine or nanoparticle as transfection agent. GFP expression is shown in green in the Lipofectamine panel and rhodamine fluorescence from the NP in red in the nanoparticle panel. Note, Rhodamine from nanoparticles and not GFP is chosen to demonstrate that every cell in the field of view is transfected with the NPs. Cell nuclei are visualized with DAPI (blue) in all images.

Published OnlineFirst February 18, 2015; DOI: 10.1158/1535-7163.MCT-14-0970

achieving high transfection efficiency in all types of cell lines (Fig. 1B). Once the binding ratios were optimized, cytotoxicity of the nanoparticles was evaluated in 4 different cancer cell lines; MCF7, MDA-MB231 (both adherent), COLO205 (semiadherent), and Jurkat (nonadherent) along with the human cell line HEK293 and mouse cell line NIH-3T3 as controls (Supplementary Fig. S2). This study ascertained that nanoparticle concentrations up to 300 μg/mL did not induce any significant cytotoxicity on the cell lines investigated. A major concern of all nanoparticulate agents in translational research is their potential toxicity *in vivo* and as a result it was important to carefully assess the biodistribution and toxicity profile of our nanoparticles *in vivo* before validating therapeutic efficacy. The reticuloendothelial system (RES) is primarily involved in the identification, biodegradation, and removal of foreign particulate matter in the body. A thorough investigation of the fate of the key organs involved in RES after treatment with the nanoparticles was performed using standard techniques such as Fourier Transform Infrared spectroscopy (FTIR) and Liver function tests (21). Histologic data obtained by hematoxylin and eosin staining of control tissue (no nanoparticles) compared with tissue from mice acutely treated for 6 weeks on weekdays with a dose of 1,250 μg (or 50 mg/kg) nanoparticles showed integrity in liver, spleen, and kidney (Supplementary Fig. S3A). This was further supported by FTIR analysis of the respective organs following treatment with the same dose of the nanoparticles (Supplementary Fig. S3B). Finally, liver function tests between control and nanoparticle-treated mice showed no significant difference with respect to the enzymes alanine transaminase or alkaline phosphatase following prolonged treatment with 1,250 μg nanoparticles (Supplementary Fig. S3C).

Efficient induction of RNA interference *in vitro*

Achieving high levels of transfection using nonviral agents remains a challenge in most semiadherent and nonadherent cell lines, due to the lack of syndecans, unlike in adherent cells (22). The majority of transfection reagents currently available for RNAi delivery show maximum efficiencies of 60% to 70% in normal adherent cell lines such as HEK293, and 20% to 30% in refractory cell lines such as NIH3T3 and cancer cell lines, including MDA-MB231 and MCF7. Semiadherent cell lines (e.g., COLO 205) and nonadherent cell lines (e.g., Jurkat) continue to be difficult to successfully transfect with commercial reagents (23). Electroporation is considered the only alternative to transfect semiadherent and nonadherent cells, although with limited success and little potential for clinical translation. The ability of our nanoparticles to transfect different types of cancer cell lines well below the toxicity level was assessed. To test the functional and practical utility of the nanoparticles, small RNA and DNA molecules, along with larger plasmid shRNAs, were employed for silencing different target genes by RNAi. The recovery/knockdown of different target proteins was analyzed *in vitro* using different types of nucleic acids in combination with the nanoparticles. miRNAs are 22–23 nt RNA molecules which predominantly bind to the 3′-UTR of the target mRNA, resulting in knockdown of target gene expression (24). To test the ability of the nanoparticles to efficiently deliver miRNAs, transfection studies were done using various mimics and knockdown probes of human miRNAs (miR-200c, miR-105, miR-432*, miR-659, miR-662, miR-921, and antimiR-21) in different cell lines. Efficient modulation of their corresponding target genes (*p53*, *β-catenin*, and *caspase 3*) was observed using immunoblotting (Fig. 2A and Supplementary Fig. S4). The ability of our nanoparticles to transfect a large DNA construct was tested by using a pGIPZ vector encoding shRNA against the ubiquitous *GAPDH* gene as a positive control and scrambled shRNA as negative control. Successful transfection of the cells was indicated by the knockdown of the target gene in all three cell lines investigated (Fig. 2B). Similarly, knockdown of the target oncogene *c-Myc* was observed when pGIPZ vector coding for *c-Myc* shRNA was used, demonstrating the effective knockdown of the target *c-Myc* oncogene as verified by qPCR, immunoblotting, and ICC (Fig. 2C).

Suppression of autochthonous mammary tumors

In the *Blg-cre Brca2/p53* conditional knockout breast cancer model, mice develop spontaneous mammary tumors between 6 and 15 months of age (Fig. 3A). Injections to the periphery of tumors were carried out using *c-Myc* shRNA (pGIPZ vector) complexed with PEI-PGMA (25:1, N:D) in a cohort of 6 mice, along with appropriate control cohorts ($n = 6$), to test the penetrability and distribution of the NPs in the tumor and the efficacy of treatment (Fig. 3B). Tumors treated with shRNA bound to the nanoparticles showed a markedly reduced tumor growth rate compared with controls (Fig. 3C). The median survival of the cohort treated with *c-Myc* shRNA-NP complex was over 30 days, compared with control cohorts that had median survivals of between 10 and 14 days (Fig. 3D). A concomitant 30-fold reduction in *c-Myc* levels was confirmed by qPCR, immunoblotting analysis, and ICC for the *c-Myc* shRNA bound to the nanoparticle treatment group in comparison with both wild-type and untreated cohorts (Fig. 3E–G). Importantly, although injection was done at the tumor periphery, equal distribution of nanoparticles was observed throughout the tumor core and extended periphery by MRI and fluorescent confocal analysis, confirming effective penetration of these complexes throughout the tumor 24 hours after injection (Supplementary Fig. S5A and S5B). In addition, no trace of the nanoparticles was observed in off-target organs even at the end of treatment, as assessed by fluorescence (Supplementary Fig. S5C and S5D).

Suppression of colorectal cancer model

In our colorectal cancer model, induction of *Apc* loss by 4-OHT and β-naphthoflavone injection results in the development of a widespread, aggressive *c-Myc*–dependent "crypt progenitor" phenotype. This mimics early tumor development along the entire length of the small intestine and results in the death of the animals within 7 to 10 days. We hypothesized that the high buffering capacity of the multiple PEI chains on the nanoparticles would render significant protection to the shRNA from the harsh environment of the gastrointestinal tract. In addition, the adhesive property of the cationic polymer with the proteoglycan-coated proteins, coupled with the ability of PEI to effect endocytosis, would result in significant transfection in the distal large intestine. Therapy was orally administered to a cohort of 6 mice, and the response was again compared with approriate control cohorts ($n = 6$). Confocal imaging tracked the presence of the nanoparticles all along the intestinal tract, with higher doses localized within the distal large intestine and comparatively only trace amounts observed in the small intestine and proximal large intestine (Fig. 4A). Despite the disproportionate presence of the nanoparticles in these tissues, effective *c-Myc* transcript and protein level reduction was observed by both qPCR and Western blotting across these major components of the gastrointestinal tract (Fig. 4C). The high

Published OnlineFirst February 18, 2015; DOI: 10.1158/1535-7163.MCT-14-0970

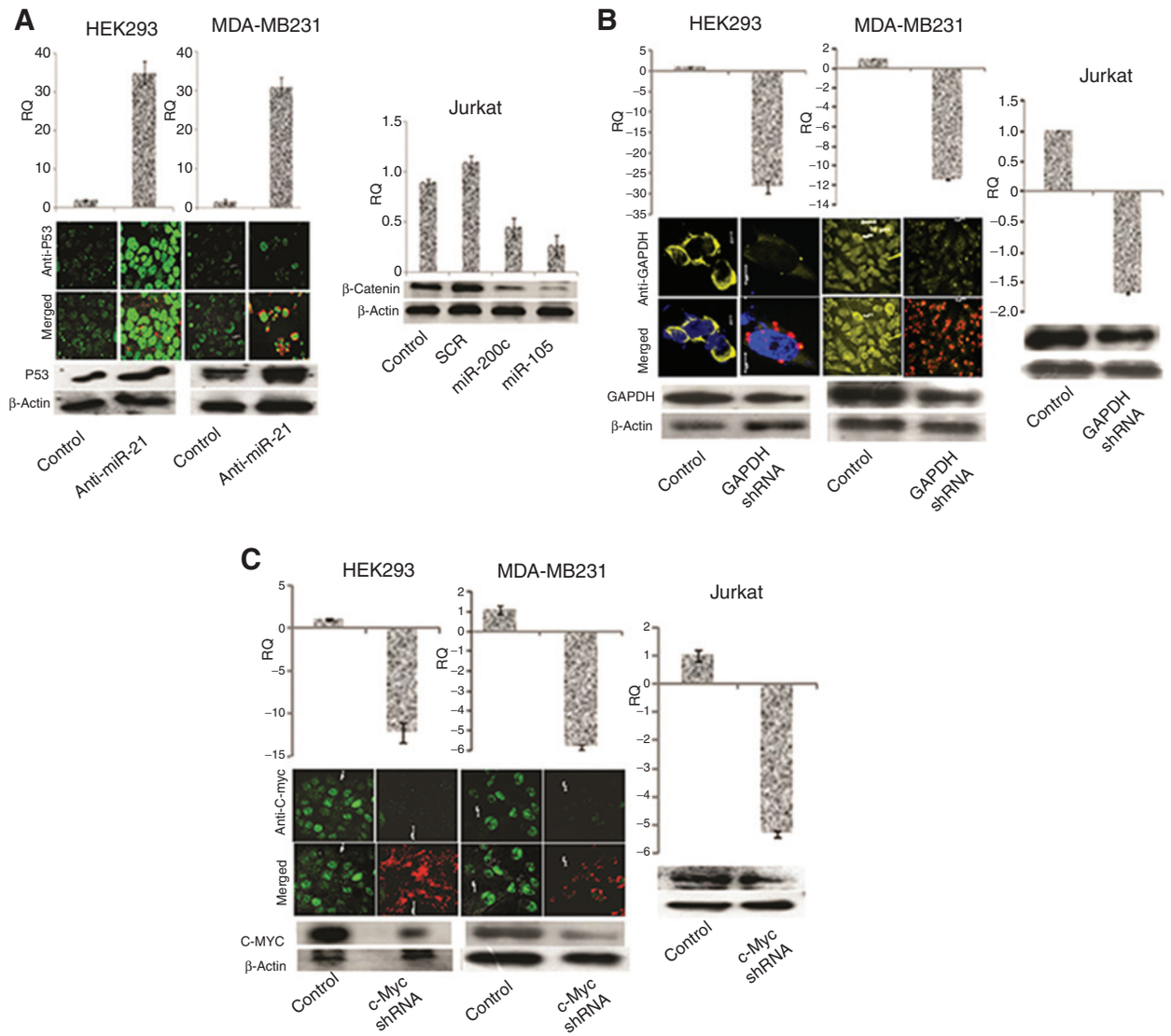

Figure 2.
Silencing of target genes using RNAi. A, upregulation of *p53* using anti-miR-21 oligos linked to the rhodamine-labeled NPs. RNAi effect of miR-21 is demonstrated by upregulation of *p53* mRNA by qPCR and protein by immunofluorescence and immunoblotting, respectively, in HEK293 and MDA-MB231 cell lines, as compared with untreated control cell lines or scrambled shRNA–treated controls. Similarly, knockdown of *β-catenin* by mimics of miR-200c and miR-105 is demonstrated by immunoblotting in Jurkat cell lines. B, downregulation of GAPDH using GAPDH shRNA linked to the nanoparticles. RNAi effect of delivered shRNA on GAPDH expression is demonstrated by qPCR, immunofluorescence and immunoblotting in HEK293, MDA-MB231, and Jurkat cell lines as compared with controls. C, knockdown of the functional oncogene *c-Myc* using *c-Myc* shRNA linked to the NPs. RNAi effect of delivered shRNA on *c-Myc* is demonstrated by qPCR, immunofluorescence, and immunoblotting in HEK293, MDA-MB231 and Jurkat cell lines as compared with controls (untreated or scrambled shRNA-treated). *β-Actin* was used as a loading control in all experiments. All qPCR experiments were conducted in triplicate, each experiment having 3 biologic replicates and 2 technical replicates, as assessed by fluorescence. The relative quantitation (RQ) of expression of the respective genes in the treated cells in relation to their respective controls is presented here. All controls were without treatment of NPs or by treating with scrambled (scr) shRNA. Representative confocal images show the Rhodamine B–labeled NPs (red), nuclei labeled with DAPI (blue), *p53, c-Myc*, and GAPDH labeled with anti-*p53*, anti-*c-Myc* (green, Alexaflour 488), and anti GAPDH (yellow), respectively. All images were captured at 10 μm scale.

levels of nanoparticles present in the large intestine is most likely a result of the timing of tissue collection and represents a snapshot of their presence in the latter stages of the normal digestive process. The cohort of animals which received oral treatment with the shRNA conjugated to the nanoparticles showed a remarkable increase in survival (median survival greater than 40 days) when compared with control cohorts, where median survival was less than 15 days in all cases (Fig. 4B). Immunohistochemical analysis at various time points throughout the treatment reflected a progressive reduction in the expression levels of the C-MYC protein (Fig. 4D). In addition, relocalization of *β-catenin* from nucleus to cytoplasm was observed during treatment, indicating a return to a non–*wnt*-deregulated state (Fig. 5A). Site triggering of the nanoparticles in the distal large intestine was shown by

Published OnlineFirst February 18, 2015; DOI: 10.1158/1535-7163.MCT-14-0970

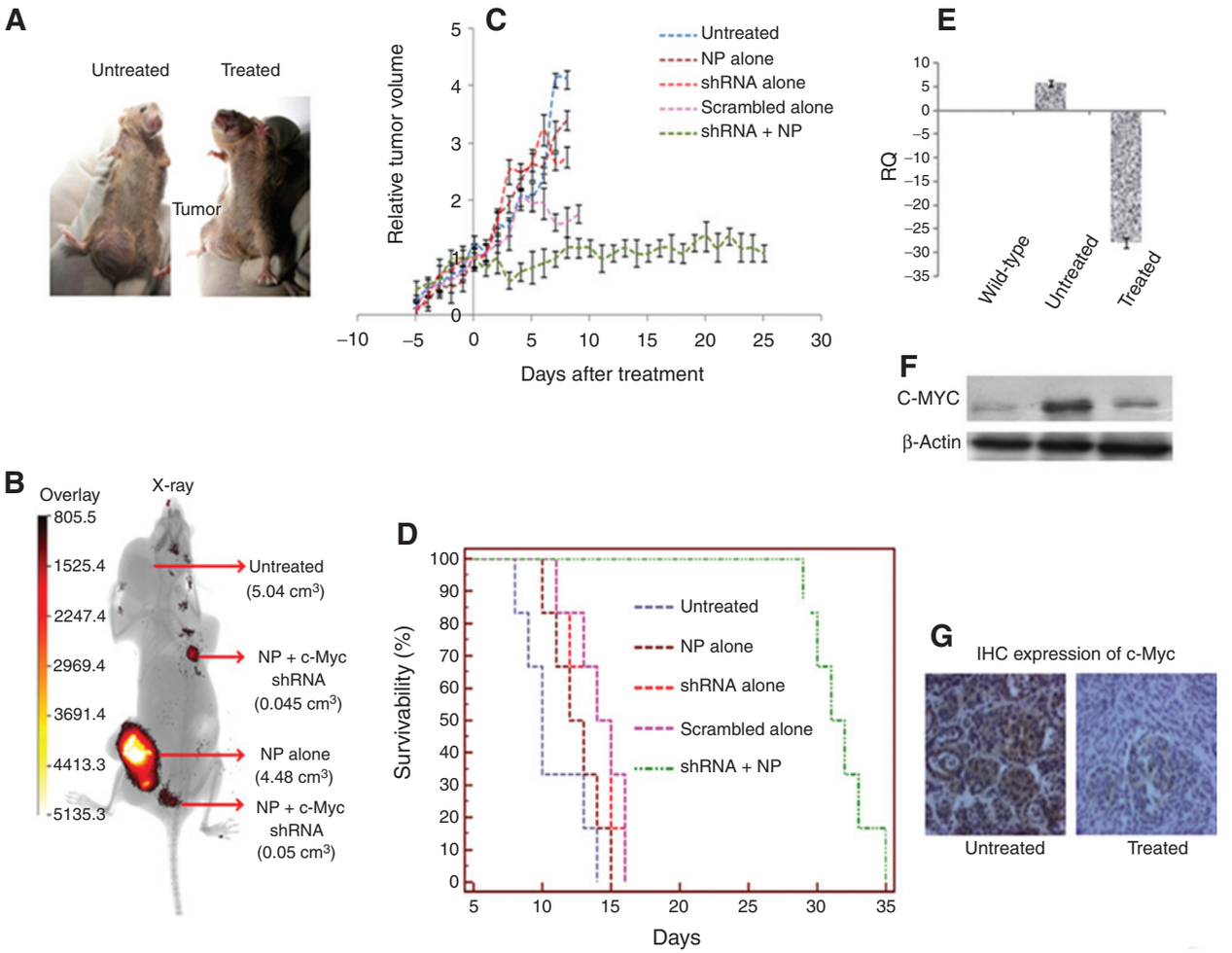

Figure 3.
Suppression of autochthonous mammary tumors by in-site delivery of nanoparticles to a mouse model of breast cancer (*Brca2/p53* knockout). A, example of mammary tumor regression in conditional *Brca2/p53* knockout mouse model upon treatment with *c-Myc* shRNA complexed with nanoparticles (NP). B, for the purpose of live multispectral imaging, 4 similarly sized mammary tumors that appeared within a span of 10 days on the same mouse were treated individually for a period of 25 days, resulting in suppression of tumors treated with *c-Myc* shRNA linked-nanoparticles (3rd and 5th mammary) compared with continued growth of untreated tumor (1st mammary) and tumor treated with scrambled shRNA-linked nanoparticles (4th mammary). The red/yellow color in the tumor core versus periphery shows the intensity of the rhodamine expression as shown in the intensity scale. Suppression of tumor growth (C) and increased survival (D) in mice treated with *c-Myc* shRNA-NPs, as compared with control cohorts. E–G, reduction in *c-Myc* transcript and protein expression levels in tumors from the treated cohorts compared with wild-type tissue and tumors from untreated mice as shown by RT-PCR (RQ) using TaqMan gene expression assays, Western blotting, and immunohistochemistry, respectively.

significant expression of turbo-FP colocalized with the nanoparticles as assessed by confocal analysis (Fig. 5B), as well as *ex vivo* multispectral imaging of the entire gut of the mouse following oral delivery (Fig. 5C). Protein ratios were calculated on the basis of densitometric quantification and were carried out using the GeneTools program (SynGene), with *β-actin* used for normalization (Supplementary Fig. S6).

Discussion

Cancer therapy has been moving through a slow process of development, hitherto hindered by limitations in drug targeting technologies. The focus on cancer drug development has shifted from toxic and nonspecific chemotherapeutic drugs to nontoxic and target-specific biologic drugs with reduced side effects. The discovery of RNAi technology has significantly enhanced our understanding of how gene expression can be modulated as a potential therapeutic tool and high-throughput screening method for targets against many cancers, although delivery of such therapy to autochthonous tumors still remains largely elusive (25). The efficiency of RNAi depends on the mode of delivery to the target, especially for diseases such as cancer. Solid tumors, such as those of the intestine, pancreas, and liver, are difficult to treat at their natural place of origin. The extravascular tumor tissue often has a limited blood supply that may render the core necrotic tissue inaccessible for drug penetration following intravenous administration, thus leading to suboptimal treatment and potential relapse (26). In this report, through both *in vitro* and *in vivo* studies, we have demonstrated the effective use of a simple nonviral nanoparticle, at a noncytotoxic level, for the targeted

Published OnlineFirst February 18, 2015; DOI: 10.1158/1535-7163.MCT-14-0970

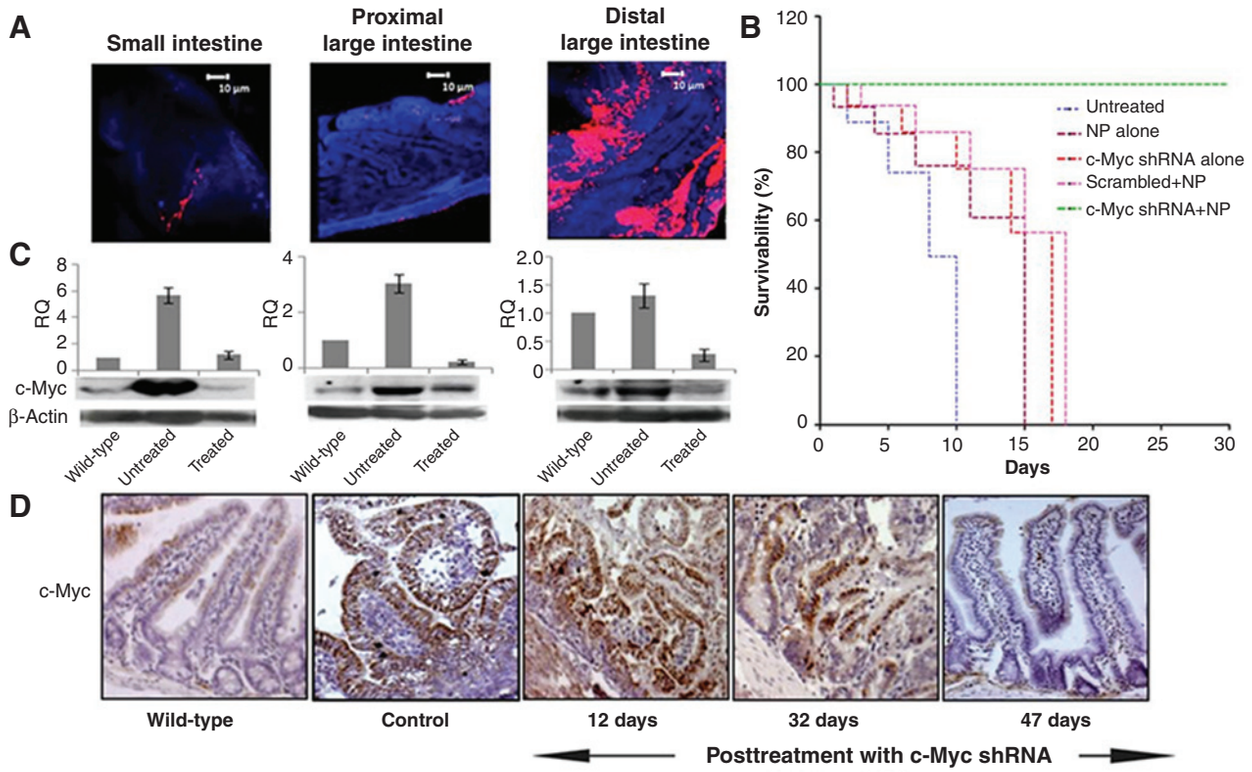

Figure 4.
Nonviral nanoparticle is suitable for oral delivery of shRNA to a mouse model of colorectal cancer (*Apc* knockout). A, confocal imaging of the fluorescent nanoparticles in *Apc*-deficient gut, following oral administration of 50 μg *c-Myc* shRNA-encoding plasmid DNA complexed with 1,250 μg nanoparticles, showing maximum retention of complex in the distal end of the large intestine. B, prolonged survival (up to 47 days) of mice treated with *c-Myc* shRNA-NP complex as compared with other treated cohorts [scrambled shRNA + nanoparticles, shRNA alone, nanoparticles alone and induced but untreated mice (control)]. Wild-type was taken as control tissue for all analyses. C, decreased *c-Myc* transcript and protein levels on 12, 32, and 47 days after treatment, as demonstrated by RT-PCR using TaqMan gene expression assays and Western blotting, respectively. Mice were healthy but culled at these timepoints specifically to analyze expression. D, immunohistochemistry for C-MYC protein in treated cohort compared with other treated groups and control cohort (as described in B), again demonstrating gradual reduction in C-MYC protein levels during treatment.

delivery of nucleic acid molecules as biologic drug cargos into different cancer tissues.

The successful transfection of the nanoparticles presented in this study is the result of PEI's ability to associate with membrane proteins, which in turn results in endocytosis of the PEI-conjugated nanoparticles. The propensity of PEI to act as a "proton sponge" allows for endosomal escape of its incorporated polyplexes. Following endocytosis, natural acidification within the endosome protonates PEI, inducing chloride ion influx, osmotic swelling, and destabilization of the vesicle, leading to the release of the polyplex into the cytoplasm. Grafting multiple PEI chains on to a macromolecular core significantly enhanced the nanoparticles capability to transfect, protect, and deliver DNA/RNA molecules. The glycidyl methacrylate units, located in the "loops" of the PGMA core with multiple free epoxy groups, serve as reactive sites for the subsequent attachment of the PEI subunits. The major difference between this method and the traditional method of anchoring PEI to the surface of a nanoparticle lies in the mobility of the epoxy functional groups located on the PGMA core. This increased mobility ensures better access to the epoxide functional groups, resulting in a 2- to 3-fold greater grafting density when compared with a monolayer of epoxy groups on a nanoparticle surface of similar dimension (27). Furthermore, the emulsification method used for the synthesis of the nanoparticle core allows for the encapsulation of magnetite (Fe_3O_4) nanoparticles within the core. The efficacy of our nanoparticle formulation was demonstrated as a nonviral agent through the high-density covalent binding of PEI onto a rhodamine B linked polyglycidal methacrylate (RhB-PGMA) reactive nanoparticle core. A polymer with epoxy functionality was chosen as the core, as the reactions of epoxy groups are quite universal, affording ease of attachment of the amino functionalized PEI and carboxylic functionalized RhB. In addition, the epoxy groups of the polymer can crosslink to provide structural integrity to the core. This renders the nanoparticles as multimodal, with rhodamine B allowing for fluorescence imaging and magnetite for MRI contrast, thus providing suitability for use in both *in vitro* and *in vivo* studies.

Our *in vitro* studies showed that nucleic acids conjugated to nanoparticles enhanced transfection efficiency and knockdown or recovery of various oncogenes and tumor suppressor genes in a number of cell lines. Using our nanoparticles, miRNAs, anti-miRs (in the form of short oligos), and larger plasmid DNAs encoding shRNAs against targeted oncogenes/tumor suppressor genes were transfected into different cancer lines at high levels of efficiency, similar to those observed with viral agents. RNAi effects of shRNAs, anti-miRs, and mimics were evident with the efficient

Published OnlineFirst February 18, 2015; DOI: 10.1158/1535-7163.MCT-14-0970

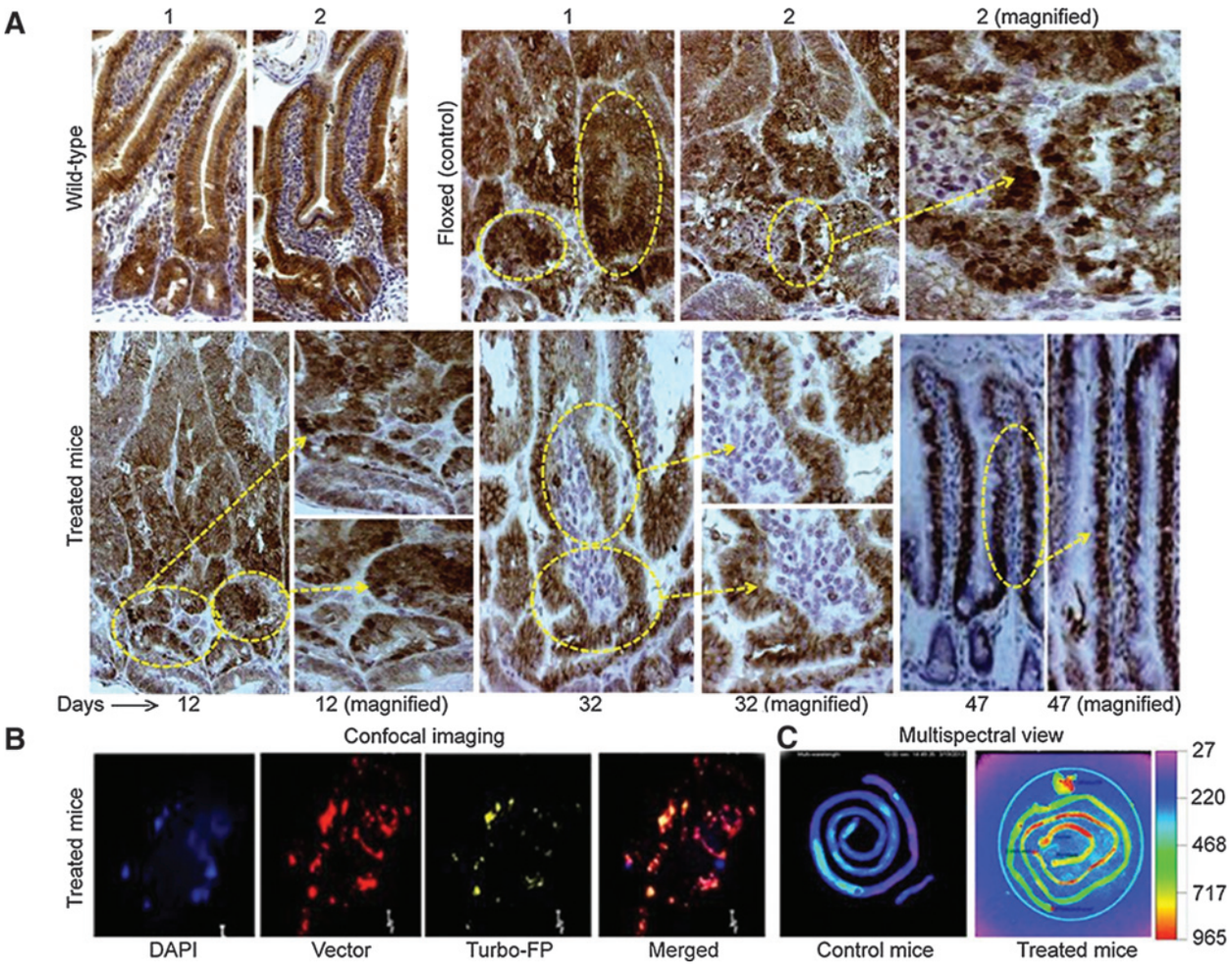

Figure 5.
Immunohistochemical analysis, reporter gene assay, and biodistribution studies on mice deleted for *Apc* in the intestine. A, *β-catenin* staining in samples from untreated wild-type, induced, and untreated, or induced and NP:*c-Myc* DNA complex-treated *apc*-deficient small intestines at various timepoints. The gut rolls were processed as described in the Materials and Methods section. Marked circles denote recombined (*apc*-deficient) areas showing dark nuclear staining (control) or fading nuclear stain with higher cytoplasmic staining in treated mice culled at different timepoints (up to 47 days). B, cryosectioning and confocal imaging of *Apc*-deficient small intestine after oral delivery of the NP:*c-Myc* DNA complex. The gut roll was made as described in Materials and Methods and immediately frozen using embedding media in dry ice for cryosectioning. These frozen gut rolls were sectioned (4–5 μm) at constant temperature (−20°C) in a Freezing Microtome and visualized using confocal microscopy at 63×. The fluorescence of rhodamine B linked to the NPs (red) and turbo-FP (reporter gene) expression (yellow) was localized within the cytoplasm, the nucleus was stained with DAPI (blue). C, *in vivo* multispectral imaging was performed to analyze the biodistribution of orally delivered nanoparticles in mice. After successive treatment for 15 days, mice were culled and the intact intestines were imaged under the multispectral imager using a rainbow filter. Comparison of the treated intestine (right) with untreated (left) shows a high level of distribution throughout the intestine.

knockdown and modulation of their respective targets. PEI-PGMA can act as a proton sponge which delays acidification and fusion with lysosome osmotic swelling and finally the rupture of some of the endosomes will in turn allow the escape of these NP–DNA complexes into the cytosol (28).

After the demonstration of effective transfection *in vitro*, we next tested the ability of c-Myc shRNA (pGIPZ) bound with nanoparticles to suppress tumors *in vivo* using an established murine transgenic *Brca2/p53*-mutant breast cancer model (19). Unlike xenografted tumor models, solid autochthonous tumors are relatively inaccessible for most treatment regimes and frequently pose challenges due to their inherent site of origin and difficulties with delivery to tumor cores. In addition, transgenic models mirror the actual mechanism of tumor progression in humans, enabling insight into the loss- or gain-of-function of genes at specific stages of tumor growth. *In vivo* in site delivery of shRNAs directly within mammary tumors enabled targeting of the extravascular tumor necrotic core, facilitating efficient knockdown of c-Myc. This genetic knockdown of a specific oncogene suppressed tumor growth effectively, thereby increasing survival, and also prevented off-target silencing in other organs. Oral delivery to mice deficient for the *Apc* gene within the intestine, allowed the encapsulated biotherapeutic to be specifically delivered to tumor-like cells therein, thus protecting it from degradation under the harsh conditions of the stomach. Again, this allowed the drug to accumulate at the right therapeutic concentration, thereby

Published OnlineFirst February 18, 2015; DOI: 10.1158/1535-7163.MCT-14-0970

triggering the inhibition of neoplastic spread. The persistent and efficient knockdown brought about by *c-Myc* shRNA returned the small intestine to a near normal state, the effect of which was translated as markedly increased survival in the treatment cohort. This anticancer drug cargo thus promises an efficient biotherapeutic regime for currently undruggable targets at problematic sites without obvious cytotoxicity. This observation has great implications for the treatment of solid tumors at their natural site of origin. A key factor that will contribute towards the successful translation of this platform will be the development of a robust, scalable production of the nanoparticle formulations in a good manufacturing practice facility, with further control over particle size distribution as described in previous polymer formulation reports (29). In the present case, we believe this is achievable by fine-tuning the emulsion polymerization process. Although we demonstrate a proof-of-principle, our approach would be further enhanced by the development of moieties that would enable targeted, site-specific delivery so as to avoid off-target effects.

In conclusion, we have demonstrated that we can use macromolecular grafting approaches to design efficient nonviral formulations that have *in vivo* capacity to deliver long-term effective RNAi therapy against cancer. Furthermore, this work also demonstrates in-site delivery of a biologic drug, for effective accumulation to therapeutic levels, the most desirable and preferred method for translation from bench to the bedside in cancer therapy.

Disclosure of Potential Conflicts of Interest

No potential conflicts of interest were disclosed.

Authors' Contributions

Conception and design: A.R. Clarke, L.D. Kumar
Development of methodology: T.D. Clemons, T. Hay, N.M. Smith, B. Zdyrko, A. Bourdoncle, I. Luzinov, K.S. Iyer, A.R. Clarke, L.D. Kumar
Acquisition of data (provided animals, acquired and managed patients, provided facilities, etc.): N.K. Tangudu, V.K. Verma, S.S. Beevi, T. Hay, G. Mahidhara, M. Raja, R.A. Nair, L.E. Alexander, A.B. Patel, J. Jose
Analysis and interpretation of data (e.g., statistical analysis, biostatistics, computational analysis): N.K. Tangudu, V.K. Verma, S.S. Beevi, T. Hay, G. Mahidhara, A.R. Clarke, L.D. Kumar
Writing, review, and/or revision of the manuscript: T.D. Clemons, T. Hay, G. Mahidhara, K.S. Iyer, A.R. Clarke, L.D. Kumar
Administrative, technical, or material support (i.e., reporting or organizing data, constructing databases): K.S. Iyer, A.R. Clarke, L.D. Kumar
Study supervision: A.R. Clarke, L.D. Kumar

Acknowledgments

The authors thank the Australian Microscopy & Microanalysis Research Facility at the Centre for Microscopy, Characterization & Analysis, and The University of Western Australia, funded by the University, State, and Commonwealth Governments. The authors thank Dr. Dinesh Kumar for help with statistical analysis and critical evaluation of the manuscript, Abdul Rawoof for helping with formatting text and figures, Prof. J.L. Mergny and Velu Mani Selvaraj for editing the manuscript, N. Mahesh Babu, and Avinash Raj for their help in tissue processing, IHC and animal handling during toxicity studies, G. Srinivas for flow cytometry analysis, Dr. E.R. Prasad and Ch. Kiran for their assistance in Western blot analysis.

Grant Support

This work was funded by Department of Science and Technology (SR/SO/HS-51-2007, Department of Biotechnology (BT/PR10024/AGR/36/28/2007) Ministry of Science and Technology, Government of India, CSIR 12th FYP- BSC 103 (to L. Dinesh Kumar and colleagues, the Australian Research Council (ARC), the National Health & Medical Research Council (NHMRC) of Australia and the National Science Foundation (CBET-0756457) as well as ANR P-NANO and F-DNA, the Conseil Régional d'Aquitaine, and Association pour la recherche sur le Cancer (ARC; to S. Iyer and colleagues). A.R. Clarke and colleagues were supported by CR-UK, the Welsh Government, and Tenovus.

The costs of publication of this article were defrayed in part by the payment of page charges. This article must therefore be hereby marked *advertisement* in accordance with 18 U.S.C. Section 1734 solely to indicate this fact.

Data and materials availability:

All reasonable requests for collaboration involving materials used in the research will be fulfilled provided that a written agreement is executed in advance between the requester (and his or her affiliated institution) and the Centre for Cellular and Molecular Biology, Council of Scientific and Industrial Research, India; The University of Western Australia, Australia and Cardiff University, UK.

Received November 7, 2014; revised February 4, 2015; accepted February 10, 2015; published OnlineFirst February 18, 2015.

References

1. Bishop JM. Retroviruses and cancer genes. Adv Cancer Res 1982;37:1–32.
2. Elend M., Eilers M. Cell Growth: Downstream of Myc - To Grow or To Cycle? Curr Biol 1999;9:R936–8.
3. Zhang L, Hou Y, Ashktorab H, Gao L, Xu Y, Wu K, et al. The impact of C-MYC gene expression on gastric cancer cell. Mol Cell Biochem 2010;344:125–35.
4. Caplen NJ. Gene therapy progress and prospects. Downregulating gene expression: the impact of RNA interference. Gene Ther 2004;11:1241–48.
5. Dykxhoorn DM, Lieberman J. The silent revolution: RNA interference as basic biology, research tool, and therapeutic. Annu Rev Med 2005;56:401–23.
6. Kumar LD, Clarke AR. Gene manipulation through the use of small interfering RNA (siRNA): From *in vitro* to *in vivo* applications. Adv Drug Deliver Rev 2007;59:87–100.
7. Kota J, Chivukula RR, O'Donnell KA, Wentzel EA, Montgomery CL, Hwang HW, et al. Therapeutic microRNA delivery suppresses tumorigenesis in a murine liver cancer model. Cell 2009;137:1005–17.
8. Li CX, Parker A, Menocal E, Xiang S, Borodyansky L, Fruehauf JH. Delivery of RNA interference. Cell Cycle 2006;5:2103–9.
9. Siolas D, Lerner C, Burchard J, Ge W, Linsley PS, Paddison PJ, et al. Synthetic shRNAs as potent RNAi triggers. Nat Biotechnol 2005;23:227–31.
10. Jensen SA, Day ES, Ko CH, Hurley LA, Luciano JP, Kouri FM, et al. Spherical nucleic acid nanoparticle conjugates as an RNAi-based therapy for glioblastoma. Sci Transl Med 2013;5:209ra152.
11. Lungwitz U, Breunig M, Blunk T, Gopferich A. Polyethylenimine-based non-viral gene delivery systems. Eur J Pharm Biopharm 2005;60:247–66.
12. Boussif O, Lezoualch F, Zanta MA, Mergny MD, Scherman D, Demeneix B, et al. A Versatile vector for gene and oligonucleotide transfer into cells in culture and *in vivo*: polyethylenimine. Proc Natl Acad Sci U S A 1995;92:7297–301.
13. Moghimi SM, Symonds P, Murray JC, Hunter AC, Debska G, Szewczyk A. A two-stage poly(ethylenimine)-mediated cytotoxicity: implications for gene transfer/therapy. Mol Ther 2005;11:990–5.
14. Grzelinski M, Urban-Klein B, Martens T, Lamszus K, Bakowsky U, Hobel S, et al. RNA interference-mediated gene silencing of pleiotrophin through polyethylenimine-complexed small interfering RNAs in vivo exerts antitumoral effects in glioblastoma xenografts. Hum Gene Ther 2006;17:751–66.
15. Breunig M, Lungwitz U, Liebl R, Goepferich A. Breaking up the correlation between efficacy and toxicity for nonviral gene delivery. Proc Natl Acad Sci U S A 2007;104:14454–9.

Published OnlineFirst February 18, 2015; DOI: 10.1158/1535-7163.MCT-14-0970

16. Evans CW, Fitzgerald M, Clemons TD, House MJ, Padman BS, Shaw JA, et al. Multimodal analysis of PEI-mediated endocytosis of nanoparticles in neural Cells. ACS Nano 2011;5:8640–8.
17. Iyer KS, Zdyrko B, Malz H, Pionteck J, Luzinov I. Polystyrene layers grafted to macromolecular anchoring layer. Macromolecules 2003;36:6519–6526.
18. Sun S, Zeng H, Robinson DB, Raoux S, Rice PM, Wang S X, et al. Monodisperse $MFe2O_4$ (M = Fe, Co, Mn) nanoparticles. J Am Chem Soc 2004;126:273–9.
19. Hay T, Matthews JR, Pietzka L, Lau A, Cranston A, Nygren AO, et al. Poly (ADP-ribose) polymerase-1 inhibitor treatment regresses autochthonous Brca2/p53-mutant mammary tumors in vivo and delays tumor relapse in combination with carboplatin. Cancer Res 2009;69:3850–5.
20. Sansom OJ, Reed KR, Hayes AJ, Ireland H, Brinkmann H, Newton IP, et al. Loss of Apc in vivo immediately perturbs Wnt signaling, differentiation, and migration. Genes Dev 2004;18:1385–90.
21. Ramesh J, Salman A, Hammody Z, Cohen B, Gopas J, Grossman N, et al. FTIR microscopic studies on normal and H-ras oncogene transfected cultured mouse fibroblasts. Euro Biophys J 2001;30:250–5.
22. Kopatz I, Remy JS, Behr JP. A model for non-viral gene delivery: through syndecan adhesion molecules and powered by actin. J Gene Med 2004;6: 769–76.
23. Zhao N, Qi J, Zeng Z, Parekh P, Chang CC, Tung CH, et al. Transfecting the hard-to-transfect lymphoma/leukemia cells using a simple cationic polymer nanocomplex. J Control Release 2012;159:104–10.
24. Issabekova A, Berillo O, Regnier M, Anatoly I. Interactions of intergenic microRNAs with mRNAs of genes involved in carcinogenesis. Bioinformation 2012;8:513–8
25. Kim D H, Rossi JJ. Strategies for silencing human disease using RNA interference. Nat Rev Genet 2007;8:173–84.
26. Chauhan VP, Stylianopoulos T, Boucher Y, Jain RK. Delivery of molecular and nanoscale medicine to tumors: transport barriers and strategies. Annu Rev Chem Biomol Eng 2011;2:281–98.
27. Tsyalkovsky V, Klep V, Ramaratnam K, Lupitskyy R, Minko S, Luzinov I. Fluorescent reactive core-shell composite nanoparticles with a high surface concentration of epoxy functionalities. Chem Mater 2008;20:317–25.
28. Sonawane ND, Szoka FC Jr, Verkman AS. Chloride accumulation and swelling in endosomes enhances DNA transfer by polyamine-DNA polyplexes. J Biol Chem 2003;278:44826–31
29. Hrkach J, Von Hoff D, Mukkaram Ali M, Andrianova E, Auer J, Campbell T, et al. Preclinical development and clinical translation of a PSMA-targeted docetaxel nanoparticle with a differentiated pharmacological profile. Sci Transl Med 2012;4:128ra39.

Published OnlineFirst February 18, 2015; DOI: 10.1158/1535-7163.MCT-14-0970

Molecular Cancer Therapeutics

RNA Interference Using *c-Myc*–Conjugated Nanoparticles Suppresses Breast and Colorectal Cancer Models

Naveen K. Tangudu, Vinod K. Verma, Tristan D. Clemons, et al.

Mol Cancer Ther 2015;14:1259-1269. Published OnlineFirst February 18, 2015.